AIAA JOURNAL
Vol. 40, No. 6, June 2002

System Identification of a Vortex Lattice Aerodynamic Model

Jer-Nan Juang*
NASA Langley Research Center, Hampton, Virginia 23681-0001
and
Denis Kholodar† and Earl H. Dowell‡
Duke University, Durham, North Carolina 27708-0300

The state-space representation of an aerodynamic vortex lattice model is considered from a classical, system identification perspective. By the use of an aerodynamic vortex model as a numerical simulator of a wind-tunnel experiment, both full-state and limited-state data or measurements are considered. Two possible approaches for system identification are presented, and modal controllability and observability are also considered. The theory then is applied to the system identification of the flow over a delta wing, and typical results are presented.

Nomenclature

A	=	state matrix
B	=	input influence matrix
b_m	=	controllability vector
C	=	output influence matrix
D	=	direct transmission matrix
$H(i)$	=	Hankel matrices
O_p	=	observability matrix
U	=	input matrix
w	=	downwash velocity
X_q	=	controllability matrix
Y_i	=	Markov parameters
Γ	=	vortex strength
δ	=	percent error
Λ	=	diagonal matrix of eigenvalues
λ_i	=	discrete-time eigenvalues
Ψ	=	matrix of eigenvectors corresponding to eigenvalue matrix, Λ
ψ_i	=	eigenvectors corresponding to eigenvalues, λ_i

Introduction

IN recent years, several studies have been conducted at Duke University of an aeroelastic delta wing system. In particular, reduced-order unsteady aerodynamic models have been used to predict the flutter, limit-cycle oscillations (LCO), and gust-forced response of such a wing. For the case of incompressible, inviscid, and irrotational flow, an unsteady vortex lattice method was used for time-domain analyses. Moreover, once such a model was created, it was used to create a reduced-order model (ROM) that allowed a reduction in the order of the vortex lattice code from a thousand degrees of freedom or more to the order of 10 degrees of freedom, while retaining essentially the same accuracy for the representation of fluid forces acting on a wing.

The development of such a vortex lattice model and a reduced-order aerodynamic model based on aerodynamic eigenmodes can be found in Ref. 1. However, the representation of unsteady aerodynamic flowfields in terms of global aerodynamic modes can be developed in a variety of ways. In Ref. 2, the authors used proper orthogonal decomposition modes and also a system identification model for a delta wing to obtain an ROM. As yet another approach, the current work studies the system identification of a vortex lattice model in greater depth, with a view to developing a methodology that can be used constructing an ROM from wind-tunnel experimental data. The vortex lattice model is used here as a test bed for a numerical experiment in a continuation of the work begun in Ref. 2.

Received 19 May 2001; revision received 25 October 2001; accepted for publication 22 November 2001.

*Principal Scientist, Structural Dynamics Branch. Fellow AIAA.
†Research Assistant, Department of Mechanical Engineering and Material Science. Member AIAA.
‡J. A. Jones Professor, Department of Mechanical Engineering and Material Science; Dean Emeritus, Pratt School of Engineering; and Director, Center for Nonlinear and Complex Systems. Fellow AIAA.

Delta Wing Vortex Model

The flow about a cantilevered half-span delta wing is assumed to be incompressible, inviscid, and irrotational. An unsteady vortex lattice method can be used to model this flow. A typical planar vortex lattice mesh for the three-dimensional flow over a wing is shown in Fig. 1. The delta wing and the wake are divided into a number of vortex elements. Point vortices are placed on the wing and in the wake at the quarter chord of the elements. At the three-quarter chord of each plate element a collocation point is placed for the downwash, and the velocity induced by the discrete vortices is set equal to the downwash (fluid vertical velocity on the wing) imposed by the prescribed delta wing motion or the gust field. Unsteady vorticity is shed into the wake and convected with the freestream velocity. The equations expressing these relationships are well described in Ref. 1.

State-Space Representation

The relationship between a vortex lattice (VL) model and a state-space model developed by system identification methods will be established in this section. For simplicity, we begin with the assumption that full-state information is given. This allows us to develop a formulation to gain basic insight before pursuing further development of the case where only partial state data are available.

Full-State Data or Measurements

The VL model can be described by[1]

$$\tilde{A}\Gamma(k+1) + \tilde{B}\Gamma(k) = \tilde{D}\boldsymbol{u}(k+1) \tag{1}$$

where $\Gamma(k+1)$ is the strength vector of the vortex at the time step $k+1$, $\tilde{A}$ and $\tilde{B}$ are aerodynamic coefficient matrices, $\tilde{D}$ is a transfer matrix for determining the relationship between the global VL mesh and the local VL mesh on the delta wing itself, and $\boldsymbol{u}$ is the downwash vector. Expressions for $\tilde{A}$, $\tilde{B}$, and $\tilde{D}$ are given in Ref. 1. Assume that there is a state-space model with state vector $\boldsymbol{x}$ in the form

$$\boldsymbol{x}(k+1) = A\boldsymbol{x}(k) + B\boldsymbol{u}(k), \qquad \Gamma(k) = C\boldsymbol{x}(k) + D\boldsymbol{u}(k) \tag{2}$$

The question then is, does Eq. (2) give the same map (relationship) as shown in Eq. (1) from $\boldsymbol{u}$ to Γ?

To answer this question, let us proceed as follows. Under the assumption that all states are measurable, the output matrix C in Eq. (2)

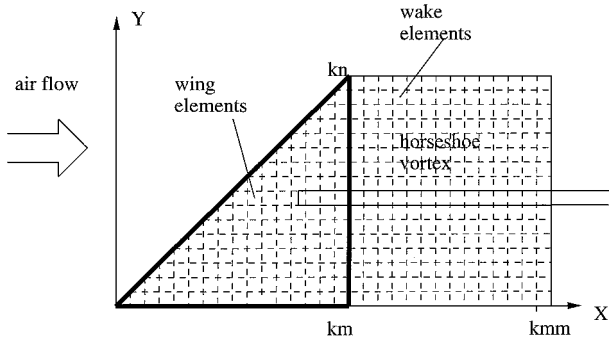

Fig. 1 Vortex lattice model of unsteady flow about a delta wing.

is square and invertible. Rewrite the bottom equation of Eq. (2) to obtain

$$\boldsymbol{x}(k) = C^{-1}\boldsymbol{\Gamma}(k) - C^{-1}D\boldsymbol{u}(k) \tag{3}$$

Substituting Eq. (3) into the top equation of Eq. (2) yields

$$C^{-1}\boldsymbol{\Gamma}(k+1) = AC^{-1}\boldsymbol{\Gamma}(k) + [B - AC^{-1}D]\boldsymbol{u}(k) + C^{-1}D\boldsymbol{u}(k+1) \tag{4}$$

Premultiplying Eq. (4) by C produces

$$\boldsymbol{\Gamma}(k+1) = CAC^{-1}\boldsymbol{\Gamma}(k) + [CB - CAC^{-1}D]\boldsymbol{u}(k) + D\boldsymbol{u}(k+1) \tag{5}$$

Comparison of Eqs. (1) and (5) results in the following equalities:

$$CAC^{-1} = -\tilde{A}^{-1}\tilde{B}, \qquad D = \tilde{A}^{-1}\tilde{D}$$
$$CB = CAC^{-1}D = -\tilde{A}^{-1}\tilde{B}\tilde{A}^{-1}\tilde{D} \tag{6}$$

From Eq. (6), it is clear that the state-space model is not unique in the sense that we have the freedom to choose C. Regardless of the choice of C, however, the eigenvalues of the VL model (i.e., eigenvalues of $-\tilde{A}^{-1}\tilde{B}$), are identical to those of A (state matrix), as long as C is invertible. For the case where C is an identity matrix, that is, $C = I$, Eq. (6) becomes

$$A = -\tilde{A}^{-1}\tilde{B}, \qquad D = \tilde{A}^{-1}\tilde{D}$$
$$B = AD = -\tilde{A}^{-1}\tilde{B}\tilde{A}^{-1}\tilde{D} \tag{7}$$

Thus, we have shown that the VL model, Eq. (1), has a state-space representation, Eq. (2), with system matrices A, B, and D, uniquely determined by Eq. (7), assuming that the output matrix C is an identity matrix. This state-space model may be used for model reduction and system identification.

Assume that we are given a (discrete time) sequence of

$$\boldsymbol{\Gamma} = [\boldsymbol{\Gamma}(1) \quad \boldsymbol{\Gamma}(2) \quad \cdots \quad \boldsymbol{\Gamma}(\ell)] \tag{8}$$

$$U = [\boldsymbol{u}(1) \quad \boldsymbol{u}(2) \quad \cdots \quad \boldsymbol{u}(\ell)] \tag{9}$$

where ℓ is the data length. This may be a sequence of experimental data obtained from measurements or, as in the present case, numerical data from the VL model. One may use these sequences $\boldsymbol{\Gamma}$ and U to identify a set of system matrices A, B, C, and D. If the identified C is an invertible square matrix, the eigenvalues of the state matrix A are, indeed, the eigenvalues of the VL model, that is, the eigenvalues of $-\tilde{A}^{-1}\tilde{B}$. To make C square and invertible requires that the number of measurements (rows) is identical to the number of states (columns). Furthermore, all rows of U must be linearly independent for the system identification to be valid. If the rows of U are not linearly independent, the matrix B cannot be properly identified. Does this mean that the eigenvalues of A may not be identified properly? The answer is no. The eigenvalues of A can be fully identified if some of the rows of U can sufficiently excite the system eigenvalues (see, for example, Ref. 3).

Limited-State Data or Measurements

For simplicity, we have first developed the basic formulation based on a set of full-state data or measurements. In practice, measurements may be extremely limited to probably a few tens of spatial locations and/or time steps. For example, what if one is given only the first few elements of $\boldsymbol{\Gamma}(k)$ for $k = 1, 2, \ldots, \ell$ generated by Eq. (1)? Can we use this very limited number of elements to identify the eigenvalues of $-\tilde{A}^{-1}\tilde{B}$? One might intuitively conclude that it is very difficult, if not impossible. However, in fact, some progress can be made as follows.

Let Eq. (1) be transformed to a new form in terms of modal coordinates, that is,

$$\boldsymbol{\Gamma}_m(k+1) + \Lambda\boldsymbol{\Gamma}_m(k) = \tilde{D}_m\boldsymbol{u}(k+1) \tag{10}$$

where

$$\Lambda = \Psi^{-1}[\tilde{A}^{-1}\tilde{B}]\Psi = \mathrm{diag}[\lambda_1 \quad \lambda_2 \quad \cdots \quad \lambda_n]$$
$$\boldsymbol{\Gamma}_m(k) = \Psi^{-1}\boldsymbol{\Gamma}(k), \qquad \tilde{\boldsymbol{D}}_m = \Psi^{-1}\tilde{A}^{-1}\tilde{\boldsymbol{D}}$$

The quantities $\lambda_1\ \lambda_2\ \cdots\ \lambda_n$ are the eigenvalues of the VL model, and $\psi_1\ \psi_2\ \cdots\ \psi_n$ are the corresponding eigenvectors that form the matrix Ψ. Assume that we have only one input, that is, $\boldsymbol{u}(k+1)$ in Eq. (10) is a scalar. All of the modes will be excited if the column vector $\tilde{\boldsymbol{D}}_m$ has no zero elements in it, and $\boldsymbol{u}(k+1)$ is nonzero. If some elements of $\tilde{\boldsymbol{D}}_m$ are zero, the corresponding eigenvectors will not be excited. Other inputs may be added to excite such modes, of course. The elements of $\tilde{\boldsymbol{D}}_m$ with relatively larger magnitude will excite the corresponding eigenmode to have a larger response. Assume that we have excited all of the modes by properly choosing the input locations and their excitation signal, that is, none of the columns in

$$\boldsymbol{\Gamma}_m = [\boldsymbol{\Gamma}_m(1) \quad \boldsymbol{\Gamma}_m(2) \quad \cdots \quad \boldsymbol{\Gamma}_m(\ell)]$$

is a zero vector. The output data or measurements will become

$$\boldsymbol{\Gamma} = [\boldsymbol{\Gamma}(1) \quad \boldsymbol{\Gamma}(2) \quad \cdots \quad \boldsymbol{\Gamma}(\ell)]$$
$$= \Psi[\boldsymbol{\Gamma}_m(1) \quad \boldsymbol{\Gamma}_m(2) \quad \cdots \quad \boldsymbol{\Gamma}_m(\ell)]$$

If Ψ is invertible, each row of $\boldsymbol{\Gamma}$ should include all information of the VL eigenvalues and eigenvectors. In theory, one should be able to extract the information of eigenvalues from one row of $\boldsymbol{\Gamma}$ unless there exist some repeated eigenvalues.[3]

Let us rewrite Eq. (1) to become

$$\boldsymbol{\Gamma}(k+1) = \hat{A}\boldsymbol{\Gamma}(k) + \hat{D}\boldsymbol{u}(k+1), \qquad y(k) = \hat{C}\boldsymbol{\Gamma}(k) \tag{11}$$

where

$$\hat{A} = -\tilde{A}^{-1}\tilde{B}, \qquad \hat{D} = \tilde{A}^{-1}\tilde{D}$$

and $\hat{C}$ is an $m \times n$ matrix with $m < n$. Each row of $\hat{C}$ could have a unity at one location and zeros at all other locations, so that $y(k)$ includes only the desired elements in $\boldsymbol{\Gamma}(k)$. From Eq. (11), the following matrix equation can be easily derived:

$$\begin{bmatrix} \boldsymbol{y}(k) \\ \boldsymbol{y}(k+1) \\ \vdots \\ \boldsymbol{y}(k+p-1) \end{bmatrix} = \begin{bmatrix} \hat{C} \\ \hat{C}\hat{A} \\ \vdots \\ \hat{C}\hat{A}^{p-1} \end{bmatrix} \boldsymbol{\Gamma}(k)$$
$$+ \begin{bmatrix} 0 & 0 & 0 & 0 \\ 0 & \hat{C}\hat{D} & 0 & 0 \\ \vdots & \vdots & \ddots & \vdots \\ 0 & \hat{C}\hat{A}^{p-2}\hat{D} & \hat{C}\hat{A}\hat{D} & \hat{C}\hat{D} \end{bmatrix} \begin{bmatrix} \boldsymbol{u}(k) \\ \boldsymbol{u}(k+1) \\ \vdots \\ \boldsymbol{u}(k+p-1) \end{bmatrix} \tag{12}$$

or

$$\boldsymbol{y}_p(k) = \Theta_p\boldsymbol{\Gamma}(k) + \Upsilon_p\boldsymbol{u}_p(k) \tag{13}$$

where

$$\boldsymbol{y}_p(k) = \begin{bmatrix} \boldsymbol{y}(k) \\ \boldsymbol{y}(k+1) \\ \vdots \\ \boldsymbol{y}(k+p-1) \end{bmatrix}, \qquad \boldsymbol{u}_p(k) = \begin{bmatrix} \boldsymbol{u}(k) \\ \boldsymbol{u}(k+1) \\ \vdots \\ \boldsymbol{u}(k+p-1) \end{bmatrix}$$

$$\Theta_p = \begin{bmatrix} \hat{C} \\ \hat{C}\hat{A} \\ \vdots \\ \hat{C}\hat{A}^{p-1} \end{bmatrix}, \qquad \Upsilon_p = \begin{bmatrix} 0 & 0 & 0 & 0 \\ 0 & \hat{C}\hat{D} & 0 & 0 \\ \vdots & \vdots & \ddots & \vdots \\ 0 & \hat{C}\hat{A}^{p-2}\hat{D} & \hat{C}\hat{A}\hat{D} & \hat{C}\hat{D} \end{bmatrix}$$

and p is an integer that must be chosen to make Θ_p a square matrix of $pm \times n$, with $pm = n$, and m is the number of outputs. There is a substantial chance that such an integer p does not exist. We will discuss this case later. The quantity Υ_p is a $pm \times pr$ matrix with r being the number of inputs.

The quantity $\boldsymbol{y}_p(k)$ is a $pm \times 1$ column vector stacking together the $m \times 1$ vectors, $\boldsymbol{y}(k), \boldsymbol{y}(k+1), \ldots, \boldsymbol{y}(k+p-1)$ from different time steps, where m is the number of outputs. Similarly, the quantity $\boldsymbol{u}_p(k)$ is a $pr \times 1$ column vector consisting of $r \times 1$ vectors, $\boldsymbol{u}(k), \boldsymbol{u}(k+1), \ldots, \boldsymbol{u}(k+p-1)$, where r is the number of inputs. Solving Eq. (13) for $\boldsymbol{\Gamma}(k)$ yields

$$\boldsymbol{\Gamma}(k) = \Theta_p^{-1}\boldsymbol{y}_p(k) - \Theta_p^{-1}\Upsilon_p\boldsymbol{u}_p(k) \tag{14}$$

Substituting $\boldsymbol{\Gamma}(k)$ and $\boldsymbol{\Gamma}(k+1)$ from Eq. (14) into Eq. (11) and premultiplying the resultant equation by Θ_p produces

$$\boldsymbol{y}_p(k+1) = \Theta_p\hat{A}\Theta_p^{-1}\boldsymbol{y}_p(k) - \Theta_p\hat{A}\Theta_p^{-1}\Upsilon_p\boldsymbol{u}_p(k) + \Upsilon_p\boldsymbol{u}_p(k+1) + \Theta_p\hat{D}\boldsymbol{u}(k+1) \tag{15}$$

Assume that the number of inputs is r, that is, $\boldsymbol{u}(k+1)$ is an $r \times 1$ vector. Define $\hat{\Upsilon}_p$ as

$$\hat{\Upsilon}_p = \Upsilon_p \text{ with the first } r \text{ zero columns replaced by } \Theta_p\hat{D} \tag{16}$$

Equation (15) becomes

$$\boldsymbol{y}_p(k+1) = \Theta_p\hat{A}\Theta_p^{-1}\boldsymbol{y}_p(k) - \Theta_p\hat{A}\Theta_p^{-1}\Upsilon_p\boldsymbol{u}_p(k) + \hat{\Upsilon}_p\boldsymbol{u}_p(k+1) \tag{17}$$

For easy reference, let us call Eq. (17) the generalized vortex lattice (GVL) model. This equation has a state-space representation similar to Eq. (2), that is,

$$\boldsymbol{x}(k+1) = A\boldsymbol{x}(k) + B_p\boldsymbol{u}_p(k)$$
$$\boldsymbol{y}_p(k) = C_p\boldsymbol{x}(k) + D_p\boldsymbol{u}_p(k) \tag{18}$$

where

$$A = \Theta_p\hat{A}\Theta_p^{-1}, \qquad B_p = \Theta_p\hat{A}\Theta_p^{-1}[\hat{\Upsilon}_p - \Upsilon_p]$$
$$C_p = I_{pm \times pm}, \qquad D_p = \hat{\Upsilon}_p \tag{19}$$

The output matrix C_p is chosen to be an identity matrix. Equation (18) is a state-space model representing the map from the input vector $\boldsymbol{u}_p(k)$ of $pr \times 1$ to the output vector $\boldsymbol{y}_p(k)$ of $pm \times 1$. Now we seek the map from input vector $\boldsymbol{u}(k)$ of $r \times 1$ to the output vector $\boldsymbol{y}(k)$ of $m \times 1$. Careful examination of $\hat{\Upsilon}_p$ as defined in Eq. (16) reveals that

$$\hat{\Upsilon}_p - \Upsilon_p = [\Theta_p\hat{D} \quad 0_{pm \times (p-1)r}] \tag{20}$$

where $0_{pm \times (p-1)r}$ is a $pm \times (p-1)r$ zero matrix. Equation (18), thus, reduces to

$$\boldsymbol{x}(k+1) = A\boldsymbol{x}(k) + B\boldsymbol{u}(k), \qquad \boldsymbol{y}(k) = C\boldsymbol{x}(k) + D\boldsymbol{u}(k) \tag{21}$$

where

$$A = \Theta_p\hat{A}\Theta_p^{-1}, \qquad B = \Theta_p\hat{D}$$
$$C = [I_{m \times m} \quad 0_{m \times (p-1)m}], \qquad D = \text{first } m \text{ rows of } \Theta_p\hat{D} \tag{22}$$

The measurement or data output equation for $\boldsymbol{y}(k)$ is obtained by taking the first m rows of $\boldsymbol{y}_p(k)$ shown in Eq. (18) and noting that $I_{pm \times pm}$ is an identity matrix and Υ_p is a special matrix, that is, the upper-right-hand entries are all zeros. The matrix A is related to $\hat{A}$ by a similarity transformation such that they share the same eigenvalues. We, thus, conclude that the eigenvalues for the VL model can be obtained from the state-space model shown in Eq. (21). The fundamental assumption is that the matrix Θ_p must be invertible. The matrix Θ_p is commonly referred to as the observability matrix in the control field. If some of the eigenvalues of the VL model are not observable, then Θ_p will not be full rank and, thus, not invertible. Then the identified state-space matrix A shown in Eq. (21) would not include the unobservable eigenvalues. The maximum rank of Θ_p is the number of states, n. Therefore, even though we have an oversized $pm \times n$ matrix Θ_p, with $pm > n$, a good system identification technique should be able to identify a minimum-size matrix A that would include only the observable and controllable VL eigenvalues and eigenvectors.

System Identification

Several methods may be used for system identification.[3] Each has its own disadvantages and advantages. Here, two relatively simple approaches are presented: 1) the GVL model identification and 2) the eigensystem realization algorithm (ERA).

GVL Model Identification

The GVL model identification begins with Eq. (17). Let us rewrite Eq. (17) to become

$$\boldsymbol{y}_p(k+1) = A\boldsymbol{y}_p(k) - A\Upsilon_p\boldsymbol{u}_p(k) + \hat{\Upsilon}_p\boldsymbol{u}_p(k+1) \tag{23}$$

where the state matrix A is defined in Eq. (22). Let the time index k run from 1 to ℓ. Equation (17) will then produce the following matrix equation:

$$Y_p(2) = AY_p(1) - A\Upsilon_pU_p(1) + \hat{\Upsilon}_pU_p(2)$$

or

$$Y_p(2) = [A \quad -A\Upsilon_p \quad \hat{\Upsilon}_p]\begin{bmatrix} Y_p(1) \\ U_p(1) \\ U_p(2) \end{bmatrix} \tag{24}$$

where $Y_p(1)$, $Y_p(2)$, $U_p(1)$, and $U_p(2)$ are defined by

$$Y_p(k) = [\boldsymbol{y}_p(k) \quad \boldsymbol{y}_p(k+1) \quad \cdots \quad \boldsymbol{y}_p(\ell-p+k-1)]$$
$$= \begin{bmatrix} \boldsymbol{y}(k) & \boldsymbol{y}(k+1) & \cdots & \boldsymbol{y}(\ell-p+k-1) \\ \boldsymbol{y}(k+1) & \boldsymbol{y}(k+2) & \cdots & \boldsymbol{y}(\ell-p+k) \\ \vdots & \vdots & \ddots & \vdots \\ \boldsymbol{y}(k+p-1) & \boldsymbol{y}(k+p) & \cdots & \boldsymbol{y}(\ell+k-2) \end{bmatrix}$$

$$U_p(k) = [\boldsymbol{u}_p(k) \quad \boldsymbol{u}_p(k+1) \quad \cdots \quad \boldsymbol{u}_p(\ell+p+k-1)]$$
$$= \begin{bmatrix} \boldsymbol{u}(k) & \boldsymbol{u}(k+1) & \cdots & \boldsymbol{u}(\ell-p+k-1) \\ \boldsymbol{u}(k+1) & \boldsymbol{u}(k+2) & \cdots & \boldsymbol{u}(\ell-p+k) \\ \vdots & \vdots & \ddots & \vdots \\ \boldsymbol{u}(k+p-1) & \boldsymbol{u}(k+p) & \cdots & \boldsymbol{u}(\ell+k-2) \end{bmatrix}$$

with $k = 1$ and 2. Note that A is an $n \times n$ matrix, $A\Upsilon_p$ is an $n \times pr$ matrix, and $\hat{\Upsilon}_p$ is also an $n \times pr$ matrix. Correspondingly, $Y_p(1)$

and $Y_p(2)$ are both $pm \times (\ell - p)$ matrices and $U_p(1)$ and $U_p(2)$ are both $pr \times (\ell - p)$ matrices. Note that $n = pm$ is assumed.

In Eq. (24), we have three matrices, A, $A\Upsilon_p$, and $\hat{\Upsilon}_p$, with a total of $n \times (n + 2pr)$ unknowns to be determined. The matrix

$$\begin{bmatrix} Y_p(1) \\ U_p(1) \\ U_p(2) \end{bmatrix}$$

is of the size $(n + 2pr) \times (\ell - p)$. If the data length ℓ is given such that $\ell - p \geq n + 2pr$, then the maximum rank of the matrix is $n + 2pr$ if all of the rows are linearly independent. Unfortunately, the matrices $U_p(1)$ and $U_p(2)$ have all rows in common except the first row of $U_p(1)$ and the last row of $U_p(2)$. This means that the three matrices, A, $A\Upsilon_p$, and $\hat{\Upsilon}_p$ cannot be solved uniquely. To solve the state matrix uniquely, let us define

$$\hat{\Upsilon} = [0_{n \times r} \quad -A\Upsilon_p] + [\hat{\Upsilon}_p \quad 0_{n \times r}] \tag{25}$$

By the use of Eq. (25), Eq. (24) can be rearranged to become

$$Y_p(2) = [A \quad \hat{\Upsilon}] \begin{bmatrix} Y_p(1) \\ U_{p+1}(1) \end{bmatrix} \tag{26}$$

The matrix $U_{p+1}(1)$ is the union of $U_p(1)$ and $U_p(2)$, that is, the $U_p(1)$ plus the last r row of $U_p(2)$. Now, assume that an input signal is generated such that all rows of $U_{p+1}(1)$ are linearly independent, and the resulting $Y_p(1)$ from the measurement also has linearly independent rows. Equation (26) can then be solved to yield

$$[A \quad \hat{\Upsilon}_p] = Y_p(2) \begin{bmatrix} Y_p(1) \\ U_{p+1}(1) \end{bmatrix}^{\dagger} \tag{27}$$

where the symbol † means pseudoinverse. This is a least-squares solution if

$$\begin{bmatrix} Y_p(1) \\ U_{p+1}(1) \end{bmatrix}$$

has more columns than rows.

Equation (27) provides the state matrix A as shown in Eq. (22), which, in turn, produces the eigenvalues of the VL model. Furthermore, Eq. (27) also produces the input matrix B shown in Eq. (22) that is the first r columns of $\hat{\Upsilon}_p$ [see Eqs. (16) and (22)]. Finally, the direct transmission term D is the first m rows of B [see Eq. (22)].

Equation (27) for system identification is straightforward and intuitive. Nevertheless, it does not work for the case where the data length is so short that

$$\begin{bmatrix} Y_p(1) \\ U_{p+1}(1) \end{bmatrix}$$

has more rows than columns, that is, more spatial measurement points than time steps. This pathological case is not likely to arise in practice, however. On the other hand, the state matrix A produced by Eq. (23) will, in general, not be a minimum realization in the sense that it is oversized. In other words, the integer p that produces the row number of $Y_p(1)$ and $U_{p+1}(1)$ may be chosen larger than the number of states.

ERA

Another approach that produces a minimum-size model is based on the minimum realization theory. This approach uses a sequence of responses generated by a pulse input to the real system or the inverse of the system transfer functions obtained from the input and output data (see Chapters 5 and 6 of Ref. 3). Let $\boldsymbol{u}_i(0) = 1, i = 1, 2, \ldots, r$, and $\boldsymbol{u}_i(k) = 0, k = 1, 2, \ldots,$ be substituted into Eq. (21). When the substitution is performed for each input element $\boldsymbol{u}_i(0) = 1, i = 1, 2, \ldots, r$, the results can be assembled into a pulse response matrix Y with dimension m by r as follows:

$$Y_0 = D, \qquad Y_1 = CB, \qquad Y_2 = CAB, \ldots, \qquad Y_k = CA^{k-1}B \tag{28}$$

The constant matrices in the sequence are known as Markov parameters (see Ref. 3).

System identification begins by forming the generalized Hankel matrix $H(0)$, composed of the Markov parameters

$$H(0) = \begin{bmatrix} Y_1 & Y_2 & \cdots & Y_q \\ Y_2 & Y_3 & \cdots & Y_{q+1} \\ \vdots & \vdots & \ddots & \vdots \\ Y_p & Y_{p+1} & \cdots & Y_{p+q-1} \end{bmatrix} \tag{29}$$

where p and q are integers. The fundamental rule is that the Hankel matrix must be formed such that its rank is larger than the order of the system to be identified. In theory, the Hankel matrix $H(0)$ and the state-space model are related by

$$\begin{aligned} H(0) &= \begin{bmatrix} Y_1 & Y_2 & \cdots & Y_q \\ Y_2 & Y_3 & \cdots & Y_{q+1} \\ \vdots & \vdots & \ddots & \vdots \\ Y_p & Y_{p+1} & \cdots & Y_{p+q-1} \end{bmatrix} \\ &= \begin{bmatrix} C \\ CA \\ \vdots \\ CA^{p-1} \end{bmatrix} [B \quad AB \quad \cdots \quad A^{q-1}B] \end{aligned} \tag{30}$$

To determine A, B, and C, first decompose the matrix $H(0)$ by using singular value decomposition to yield

$$\begin{aligned} H(0) = U\Sigma V^T &= [U_r \quad U_t] \begin{bmatrix} \Sigma_r & 0 \\ 0 & \Sigma_t \end{bmatrix} [V_r \quad V_t]^T \\ &= U_r \Sigma_r V_r^T + U_t \Sigma_t V_t^T \\ &\approx U_r \Sigma_r V_r^T \\ &= \left[U_r \Sigma_r^{\frac{1}{2}} \right] \left[\Sigma_r^{\frac{1}{2}} V_r \right] \end{aligned} \tag{31}$$

where U and V are orthonormal matrices such that $U^T U = I$ and $V^T V = I$, and Σ_t is a diagonal matrix containing the singular values that are negligible in comparison with those in the diagonal matrix Σ_r. Comparison of Eqs. (30) and (31) establishes the following equalities:

$$\begin{aligned} C &= \text{first } m \text{ rows of } \left[U_r \Sigma_r^{\frac{1}{2}} \right] \\ B &= \text{first } r \text{ columns of } \left[\Sigma_r^{\frac{1}{2}} V_r \right] \end{aligned} \tag{32}$$

The equalities in Eq. (32) are not unique, but they are balanced because both share the matrix Σ equally. To determine the state matrix A, another Hankel matrix must be formed, that is,

$$H(1) = \begin{bmatrix} Y_2 & Y_3 & \cdots & Y_{q+1} \\ Y_3 & Y_4 & \cdots & Y_{q+2} \\ \vdots & \vdots & \ddots & \vdots \\ Y_{p+1} & Y_{p+2} & \cdots & Y_{p+q} \end{bmatrix} \tag{33}$$

This matrix is formed by deleting the first column of $H(0)$ and adding a new column at the end of the matrix. As a result, $H(1)$ has the following relationship with the system matrices A, B, and C:

$$H(1) = \begin{bmatrix} Y_2 & Y_3 & \cdots & Y_{q+1} \\ Y_3 & Y_4 & \cdots & Y_{q+2} \\ \vdots & \vdots & \ddots & \vdots \\ Y_{p+1} & Y_{p+2} & \cdots & Y_{p+q} \end{bmatrix}$$

$$= \begin{bmatrix} C \\ CA \\ \vdots \\ CA^{p-1} \end{bmatrix} A[B \quad AB \quad \cdots \quad A^{q-1}B] \tag{34}$$

Substituting Eq. (31) into Eq. (34), thus, yields

$$A = \left[U_r \Sigma_r^{\frac{1}{2}}\right]^{\dagger} H(1) \left[\Sigma_r^{\frac{1}{2}} V_r\right]^{\dagger} = \Sigma_r^{-\frac{1}{2}} U_r^T H(1) V_r^T \Sigma_r^{-\frac{1}{2}} \tag{35}$$

The orthonormal property of U and V shown in Eq. (31) has been used to derive Eq. (35).

Assume that the state matrix A of order n has a complete set of linearly independent eigenvectors $\psi_1, \psi_2, \ldots, \psi_n$ with corresponding eigenvalues $\lambda_1, \lambda_2, \ldots, \lambda_n$, which are not necessarily distinct. Define Λ as the diagonal matrix of eigenvalues and Ψ as the matrix of eigenvectors, that is,

$$\Lambda = \begin{bmatrix} \lambda_1 & & & \\ & \lambda_2 & & \\ & & \ddots & \\ & & & \lambda_n \end{bmatrix} \tag{36}$$

$$\Psi = [\psi_1 \quad \psi_2 \quad \cdots \quad \psi_n] \tag{37}$$

The identified A, B, and C can then be transformed to become Λ, $\Psi^{-1}B$, and $C\Psi$. The state-space model, Eq. (21), in modal coordinates, becomes

$$\boldsymbol{x}_m(k+1) = \Lambda \boldsymbol{x}_m(k) + B_m \boldsymbol{u}(k)$$

$$\boldsymbol{y}(k) = C_m \boldsymbol{x}_m(k) + D\boldsymbol{u}(k) \tag{38}$$

where

$$\Lambda = \Psi^{-1} A \Psi, \qquad \boldsymbol{x}_m(k) = \Psi^{-1} \boldsymbol{x}(k)$$

$$B_m = \Psi^{-1} B, \qquad C_m = C\Psi$$

The diagonal matrix Λ contains the (aerodynamic flow) modal damping rates and the damped natural frequencies. The matrix $B_m = \Psi^{-1}B$ defines the initial modal amplitudes and the matrix $C_m = C\Psi$ the mode shapes at the sensor points. All of the modal parameters of a dynamic system can, thus, be identified by the three matrices Λ, $\Psi^{-1}B$, and $C\Psi$. The desired modal damping rates and damped natural frequencies are simply the real and imaginary parts of the eigenvalues Λ_c, after transformation from the discrete-time domain to the continuous-time domain using the relation

$$\Lambda_c = (1/\Delta t) \log(\Lambda) \tag{39}$$

Modal Controllability and Observability

Equation (30) shows that the Hankel matrix $H(0)$ is formed by two matrices defined by

$$O_p = \begin{bmatrix} C \\ CA \\ \vdots \\ CA^{p-1} \end{bmatrix} \tag{40}$$

$$X_q = [B \quad AB \quad \cdots \quad A^{q-1}B] \tag{41}$$

The matrix O_p is commonly called the observability matrix, whereas X_q is referred to as the controllability matrix. If the system possesses n states, both O_p and X_q may have a maximum rank of n, assuming that the integers p and q are sufficiently large. Note that O_p and X_q may not share the same rank. If either O_p or X_q is short of rank n, then some of the eigenvalues may not be identifiable. Let us elaborate on this statement by computing O_p and X_q in modal coordinates.

The matrices O_p and X_q in modal coordinates become

$$\tilde{O}_p = \begin{bmatrix} C_m \\ C_m \Lambda \\ \vdots \\ C_m \Lambda^{p-1} \end{bmatrix} = \begin{bmatrix} C\Psi \\ C\Psi[\Psi^{-1} A \Psi] \\ \vdots \\ C\Psi[\Psi^{-1} A \Psi]^{p-1} \end{bmatrix} = O_p \Psi \tag{42}$$

$$\tilde{X}_q = \begin{bmatrix} B_m & \Lambda B_m & \cdots & \Lambda^{q-1} B_m \end{bmatrix}$$

$$= [\Psi^{-1}B \quad [\Psi^{-1}A\Psi]\Psi^{-1}B \quad \cdots \quad [\Psi^{-1}A\Psi]^{q-1}\Psi^{-1}B]$$

$$= \Psi^{-1} X_q \tag{43}$$

The matrix $\tilde{O}_p$ is the modal observability matrix, whereas $\tilde{X}_q$ is the modal controllability matrix. Both matrices are coordinate dependent. Nevertheless, the Hankel matrix $H(0)$ is coordinate invariant:

$$H(0) = \tilde{O}_p \tilde{X}_q = O_p \Psi \Psi^{-1} X_q = O_p X_q \tag{44}$$

There are n columns in O_p and n rows in X_q.

Let $\boldsymbol{o}_i$ be the ith column of O_p and $\boldsymbol{c}_i^T$ the ith row of X_q. The Hankel matrix $H(0)$ can be rewritten as

$$H(0) = \tilde{O}_p \tilde{X}_q = \sum_{i=1}^{n} \boldsymbol{o}_i \boldsymbol{c}_i^T \tag{45}$$

Both $\boldsymbol{o}_i$ and $\boldsymbol{c}_i^T$ are associated with the ith eigenvalue λ_i. The matrix $H(0)$ is the sum of n rectangular matrices formed by the product of $\boldsymbol{o}_i \boldsymbol{c}_i^T$ with $i = 1, \ldots, n$. Either $\boldsymbol{o}_i$ or $\boldsymbol{c}_i^T$ will have a contribution to $H(0)$ (unless, of course, either one is a null vector). For example, if the input actuators are located at the nodes of the ith mode shapes, the row vector $\boldsymbol{c}_i^T$ is null and, thus, its norm is zero. A similar statement is also true for the output sensors and the corresponding vector $\boldsymbol{o}_i$. The degree of contribution of the system eigenvalue λ_i to $H(0)$ is determined by the product of $\boldsymbol{o}_i \boldsymbol{c}_i^T$, which yields a $pm \times qr$ matrix. The norms $\|o_i\|$ and $\|c_i\|$ are commonly used to measure the degree of observability and controllability, respectively, for the eigenvalue λ_i. On the other hand, the product $\|o_i\|\|c_i\|$ is a measure of the contribution of λ_i to $H(0)$. A relatively larger product $\|o_i\|\|c_i\|$ means easier identification of the eigenvalue λ_i from the input and output data. Note that the input signal must be rich enough in frequency to excite the controllable and observable modes to be identified.

Numerical Example

A system identification (SID) model for an unsteady aerodynamic flow has been created for several wing motions or gust excitations and corresponding aerodynamic responses. These models were derived from numerical simulations using a VL model for a delta wing with 55 vortex elements on the wing and 300 vortex elements in the wake, that is, in Fig. 1, $km = kn = 10$, and $kmm = 20$. In each case, the flow about the wing is excited by a certain type of prescribed downwash at the wing points $w(t)$.

The numerical VL model produced vortex strengths at the grid points of the wing and in the wake $\Gamma(t)$ and the corresponding pressure distribution on the wing $p(t)$. These data were then used as input for the SID model.

The following excitations to the flow have been considered: 1) step angle of attack $w(t) = \text{const}$ for $t > 0$; 2) frozen (fixed with respect to the fluid fixed coordinates) sharp-edge gust $w(t - x/v) = \text{const}$ for $(t - x/v) > 0$, where v is the airfoil or flow velocity; 3) frozen gust of changing frequency $w(t - x/v) = \text{const} \sin[\omega_{\max}(t - x/v)^2/2T]$, which is sometimes called a swept gust, where the frequency of the sweep changes from zero to the maximal frequency $\omega_{\max}$ within the period of the sweep T; 4) random downwash (w at each grid point and at every time step is a random number); and 5) frozen random gust [in which w at the first grid point (root leading-edge element) is a random number at every new

time step, such that w is then convected with the freestream velocity for the following panels during next steps].

The excitation cases 1, 2, 3, and 5 are x, or streamwise coordinate dependent only. The excitation signal at a specific location x is constant along the axis y as shown in Fig. 1. This implies that the excitation data matrices used for SID are rank deficient, that is, the rank is less than the number of inputs. The system matrices A, B, C, and D, thus identified by using these types of excitation, would not be as accurate as for those obtained from inputs with more elaborate spanwise variation. In particular, the columns in the input matrix B may not be independent. The number of independent columns in B is equal to the rank of the excitation data matrix.

On the other hand, the random excitation defined in case 4 is both x and y coordinate dependent. The excitation data matrix used for identifying the system matrices A, B, C, and D is of full rank, that is, the number of inputs, with the assumption that the excitation data length is equal to or longer than the number of inputs. The input matrix B, in particular, would be accurately identified in theory for a controllable and observable system. All columns in B are linearly independent.

Using an SID Model

The ability of an SID model obtained from one of the excitations to predict the flow for another possible excitation was studied. The aforementioned five flow excitations were considered. Results were obtained for either vortex strength data or pressure data. Consider the vortex strength data case first. Using the time histories (1000 time steps) for the downwash and the vortex strengths, where the latter was generated by the VL model for the given downwash, an SID model was obtained. That is, the state-space matrices A, B, C, and D for this particular downwash were computed. Then this SID model was used to predict the vortex strength histories due to another downwash and the results compared with the corresponding vortex strength time histories obtained by the VL model itself for that downwash. To quantify the differences between the VL and SID outputs an error δ, defined as $\delta = 100\%$, $|Q - y|/|Q|$ was used, where the norm $|X|$ is defined to be the largest singular value of X. In this case, both Q (VL vortex strengths) and y (SID predicted vortex strengths) are 1000×355 rectangular matrices (1000 time steps and 355 degrees of freedom). The same method was also used for the pressure data. These Q (VL pressure) and y (SID predicted pressure) are matrices with 1000×55 (55 elements on the wing) elements. These results are presented in Figs. 2 and 3 and in Tables 1 and 2.

In Fig. 2, the percent errors are sorted based on using the wing motion or gust excitation used to obtain an SID model, whereas the

Table 1 Percent errors using the vortex strength data

Downwash type	Step angle	Sharp edge	Swept gust	Random gust	Frozen random
Step angle, 67	0.41	3.40	246.07	84.11	79.09
Sharp edge, 50	11.64	0.00	0.21	83.90	0.00
Swept gust, 233	0.12	0.11	0.05	78.04	0.11
Random gust, 300	0.00	0.00	0.00	0.00	0.00
Frozen random, 104	13.49	0.07	0.25	89.57	0.07

Table 2 Percent errors using the pressure data

Downwash type	Step angle	Sharp edge	Swept gust	Random gust	Frozen random
Step angle, 17	0.05	4.25	168	83.8	90.7
Sharp edge, 35	20.9	0.66	0.37	320	0.65
Swept gust, 52	15.3	15.4	2.69	72.9	15.3
Random gust, 110	0.42	0.42	0.07	0.39	0.42
Frozen random, 45	25.9	1.48	0.74	290	1.46

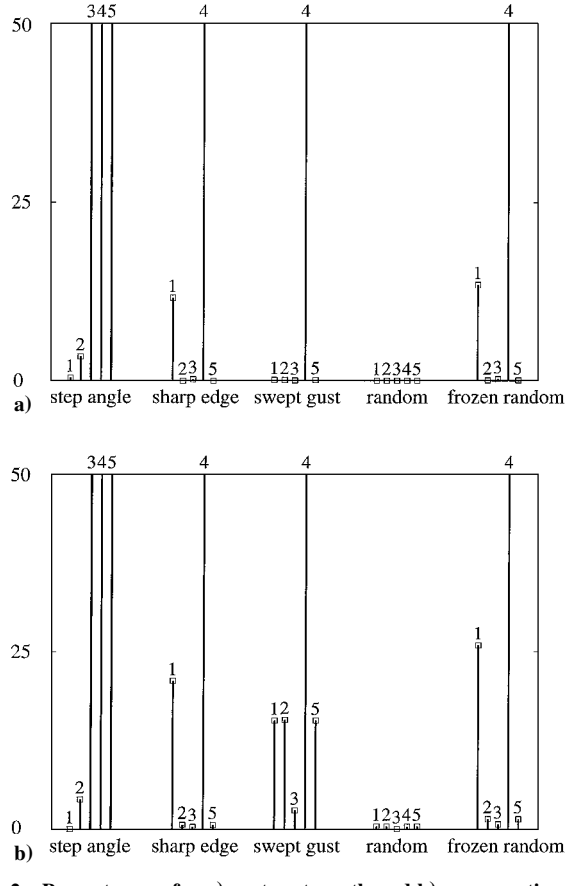

Fig. 2 Percent error for a) vortex strength and b) pressure time histories for the five described excitations (marked by the numbers); SID models used to simulate these histories are indicated along the horizontal axis, and errors correspond to how well the SID models predict time histories of different excitations.

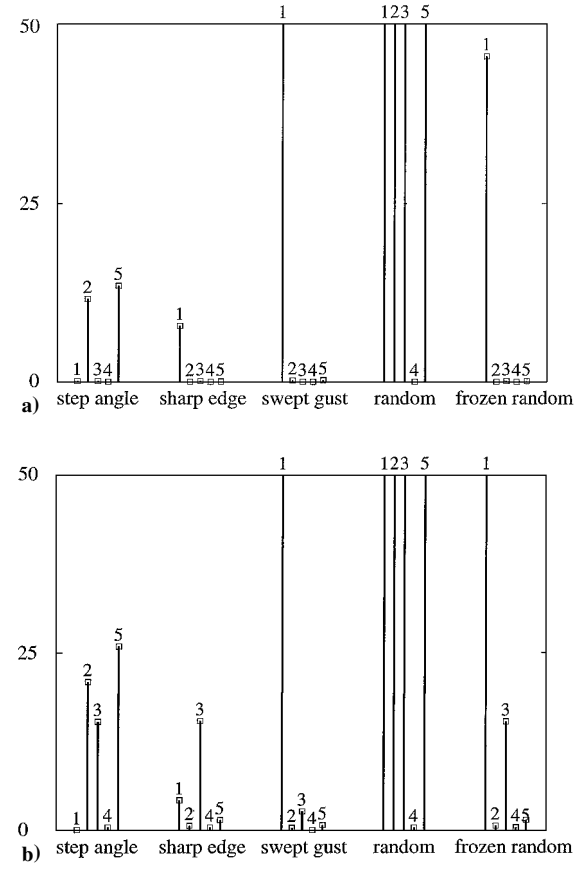

Fig. 3 Percent error for a) vortex strength and b) pressure time histories that were simulated by the SID models (marked by the numbers); flows under consideration are indicated along the horizontal axis.

errors correspond to how well that SID model predicts the vortex strength (Fig. 2a) and pressure (Fig. 2b) time histories for other excitations. A limit of 50% is used for the vertical axis scale to show small errors better. When applied to the very same downwash, the SID models compute the output with the less than 1% error (see Ref. 2). As seen in Fig. 2 for both the vortex strengths and pressure, the random excitation case is the best choice to obtain an SID model that will predict the behavior for any of the considered cases. In Fig. 2a, one can see that, if not asked to predict the very special case of a random downwash, three other models based on sharp-edge, swept gust, and frozen random excitation also work reasonably well.

The results in Fig. 3 are sorted based on the flow one is trying to predict with an SID model. For example, from Fig. 3a one can conclude that to be able to predict the vortex strengths due to a swept or frozen random gust, SID models obtained from any excitation case (except the step angle of attack excitation) would do a very good job, whereas for the prediction of vortex strengths due to a step angle of attack wing motion or sharp edge excitation, any of considered SID models would perform well. Not surprisingly (after studying Fig. 2), both Figs. 3a and 3b show that only an SID model obtained from random downwash data can predict the time history of aerodynamic flow due to the random downwash. The values of these errors are presented in Tables 1 (vortex strengths) and 2 (pressure), where the rows of Tables 1 and 2 relate to Fig. 2 and columns to Fig. 3.

It is useful to consider the number of singular values kept in the SID models. The number following the wing motion/gust designation in the first column of Tables 1 and 2 is the number of singular values retained in the identified SID model for that wing motion/gust. For the vortex strength data cases, the maximum number of singular values varies from 50 for the sharp-edge gust to 300 for the random gust. This number is chosen such that the ratio of the largest singular value to the smallest one retained was 10^{12}. For the vortex strength case, the total number of singular values is 300 (which, in fact, is equal to the total number of panels minus the number of panels on the wing). Thus, in the random gust case the signal is such that all of the singular values are relatively high and close to each other in magnitude.

Lift

As a global measure of the aerodynamic flow, consider the lift on the wing vs time. In Figs. 4a and 4b, the lift time history for the motion of the wing due to the step angle of attack is presented. In Figs. 4c and 4d, the lift time history for the excitation by the frozen sharp-edge gust is shown. (Each case is split into two figures to show in detail the predicted steady-state lift.) The solid line is the original lift (obtained from the VL model). The left-pointed and right-pointed triangles represent lift time histories from SID models obtained from the step angle of attack motion and frozen sharp-edge gust, respectively, circles, frozen swept gust; squares, random gust; and diamonds, frozen random gust. Note that the steady-state lift due to either step angle of attack or sharp-edge gust of the same amplitude is identical, which is why Fig. 4b is identical to Fig. 4d. By comparing the graphs in Fig. 4 with either results in Fig. 3b or Table 2, it can be concluded that the error norm discussed earlier does a good job of reflecting the difference between the original flow and those predicted by the identified models. However, the additional insight gained from the plots in Figs. 4b and 4d is that SID models from all excitations (but the swept gust) predict the steady-state flow very well.

From the preceding numerical results, it is clearly seen that the system response may not be reproduced using an identified model from excitations other than the random gust or its own excitation. Note that only the random gust could identify an accurate model described by the system matrices A, B, C, and D for all other inputs. Other kinds of excitation including the step angle, sharp edge, swept gust, and frozen random could only reproduce its own response, although some excitations such as swept gust may identify a model that gives a reasonable prediction for the responses produced by step angle, sharp edge, and frozen random. Nevertheless, none of the identified models produced by the step angle, sharp edge, swept

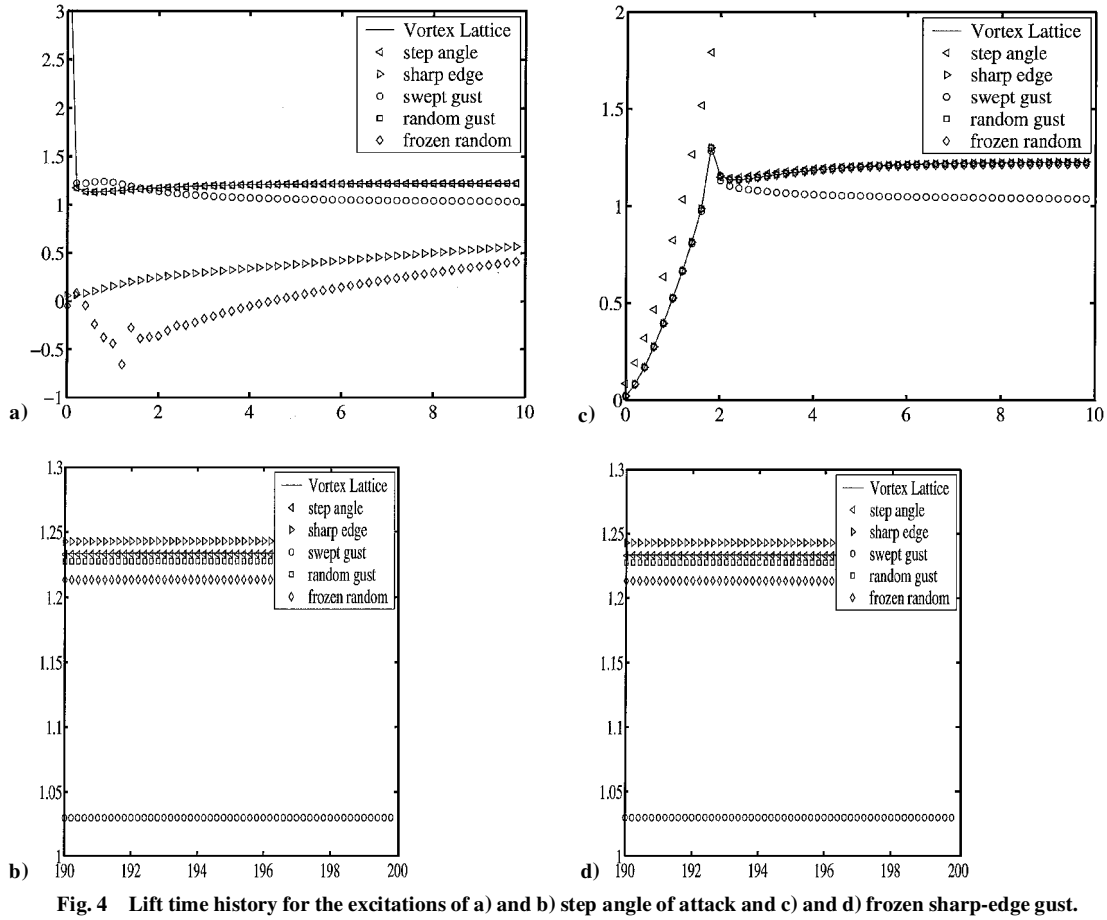

Fig. 4 Lift time history for the excitations of a) and b) step angle of attack and c) and d) frozen sharp-edge gust.

gust, and frozen random could predict the response excited by the random gust. This is because the excitations other than the random gust did not excite all system modes to identify a state-space model to represent the system accurately. Recall that only in the case of a random gust are all of the excitation (downwash) data independent, whereas in the four other cases only 10 of them are independent. (The downwash along the y coordinate is the same.) Some modes can only be excited by independent downwash along the y coordinate as well as the x coordinate.

Modal Controllability and Observability

The modal observability and controllability matrices (42) and (43) were computed for small numbers of outputs Y and inputs U, respectively. The ranks of the controllability and observability matrices ranged between 63 and 91, depending on what output and input elements were used when building O_p and X_q [Eqs. (42) and (43)]. For example, the rank of the controllability matrix in the case when there is only one input applied at the tip element of the wing (only the last column of the full input influence matrix B remains) was 91. Recall that the system has $n = 355$ states, which is the maximum rank. Therefore, because the ranks of the controllability and observability matrices are fewer than 355, the system may not be controllable and/or observable if only one input located at the tip element of the wing is used. Moreover, a controllability vector $\boldsymbol{b}_m$ (see Sec. 5.1.1 of Ref. 3) was computed. This vector is formed by the product of the inverse of the modal matrix with the eigenvectors of A as its column vectors and a column of the input influence matrix B. It was shown[3] that, if $\boldsymbol{b}_m$ has a zero element, then the control force applied at that modal node cannot control this mode. This means that the control force is acting exactly at the node of the mode.

It was found that the modes corresponding to the dominant branch of the aerodynamic flow eigenvalues (for an earlier discussion of the aerodynamic eigenvalues, see Ref. 2) are the least controllable for the input located at the tip element of the wing. The components of the vector $\boldsymbol{b}_m$ were scaled such that the largest component is one. In Fig. 5, the continuous time eigenvalues of the system are shown: In Fig. 5a those eigenvalues that have corresponding components of the controllability vector with values larger than 0.1 are noted by a cross x; in Fig. 5b, similar results are shown for 0.01. As one can see, even in the latter case, the eigenvalues of the dominant branch are still not well identified.

Values of all components of the controllability vector are shown in Fig. 6a. The mode number is plotted along the horizontal axis, whereas the vertical axis shows the value of the components of the scaled vector $\boldsymbol{b}_m$. The modes corresponding to the dominant branch of the eigenvalues are numbered from 1 to 25. These are in general complex conjugates, but note that only eigenvalues with positive frequencies are shown in Fig. 6a. Moreover, the first 10 eigenvalues are purely real and lie virtually on top of each other as shown by the single circle or data point closest to zero or the origin of the eigenvalue distribution. As seen from Fig. 6a, they are the least controllable. The same result persists if other locations of the input force are considered or, indeed, if the force is applied at more than one location, including all 55 vortex lattice panels on the wing.

An investigation of modal observability showed that the dominant modes are the most observable. Observability vector components are presented in Fig. 6b, and the continuous time eigenvalues that correspond to modes with scaled observability vectors larger than certain value are presented in Fig. 7. In Fig. 7a, the components larger than 0.4 were well identified, that is, the crosses and zeros agree. Note that the two rightmost circles corresponding to the first

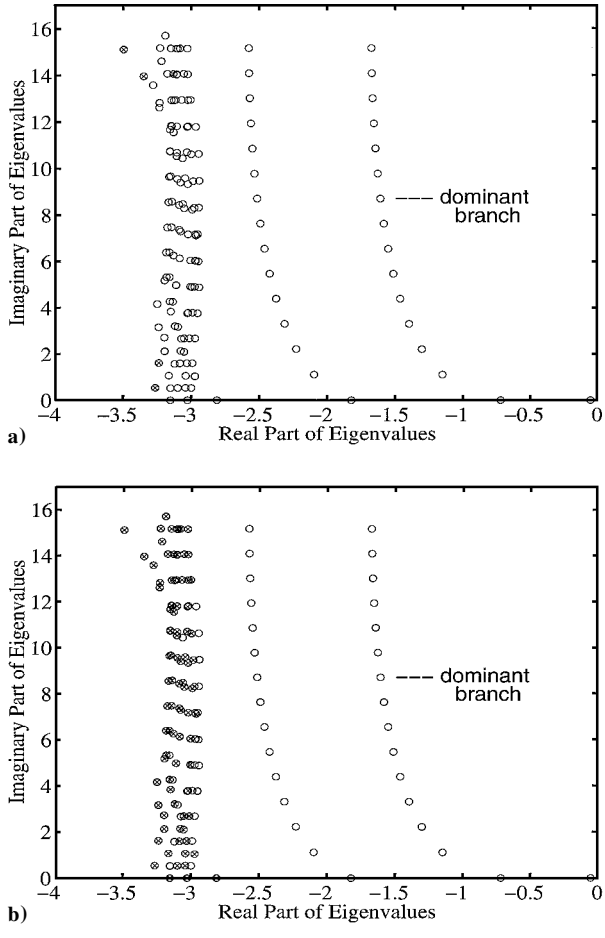

Fig. 5 System eigenvalues: Crossed eigenvalues correspond to modes for which components in the scaled controllability vector are larger than a) 0.1 and b) 0.01; largest controllability vector component is 1 (cf. Fig. 6a).

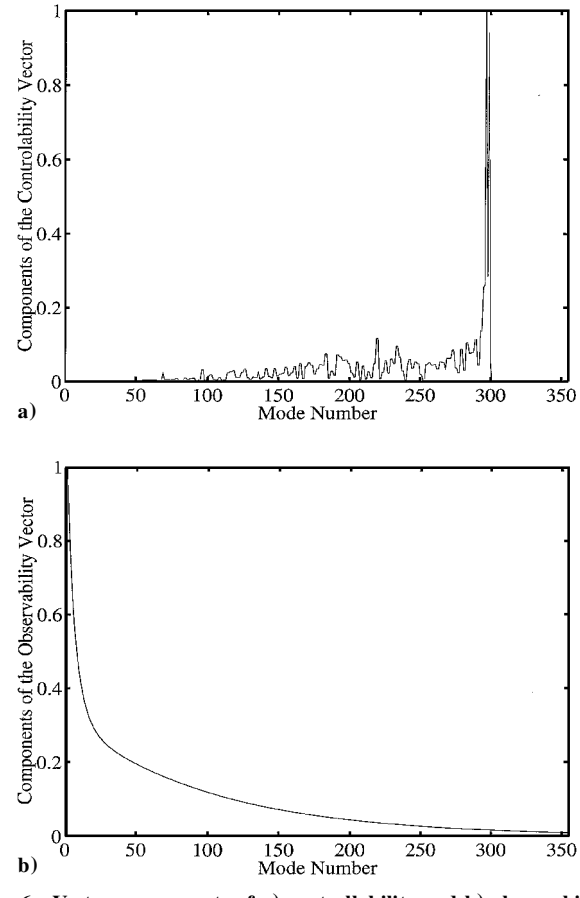

Fig. 6 Vector components of a) controllability and b) observability: Here the state A and input influence B matrices were derived in the close form from the VL model with the use of Eqs. (7), where the output influence matrix C is an identity matrix. The only input is located at the tip of the delta wing.

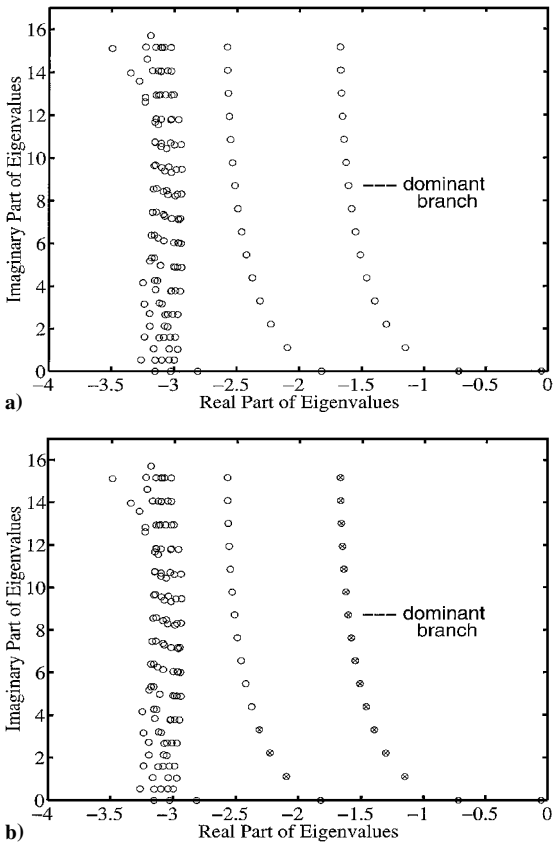

Fig. 7 System eigenvalues: Crossed eigenvalues correspond to modes for which components in the scaled observability vector are larger than a) 0.4 and b) 0.2; the largest observability vector component is 1 (cf. Fig. 6b).

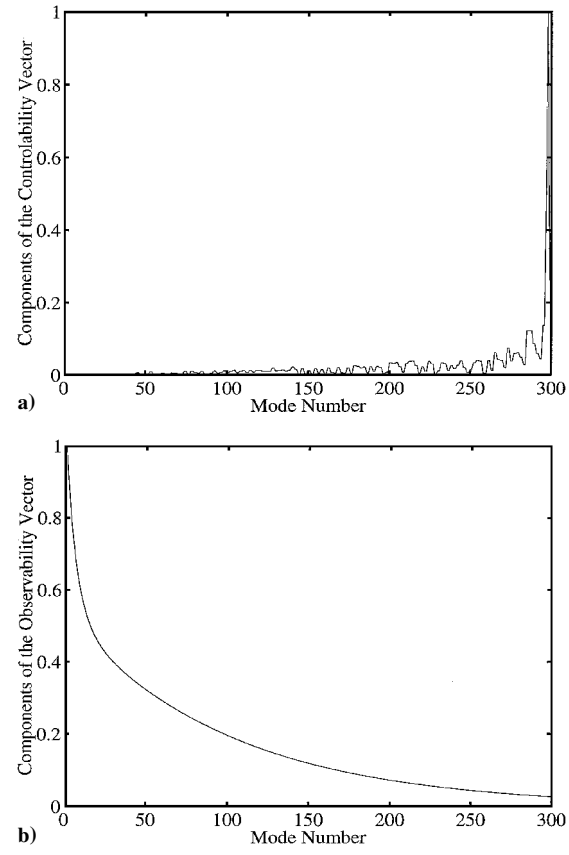

Fig. 8 Vector components for a) controllability and b) observability: Here the *A*, *B*, and *C* matrices were identified from the vortex strength data when the wing was excited by the random gust; the only input is located at the tip of the delta wing.

11 modes are crossed, and, in Fig. 7b, all of the components that are larger than 0.2 were well identified. Unlike the controllablity case, the modes that correspond to the dominant branch are the most observable.

Qualitatively, the same controllability and observability results were found when the identified system was obtained using considered excitations. Such results for the case of random gust excitation are presented in Fig. 8: The modes corresponding to the dominant branch are the least controllable (Fig. 8a) and the most observable (Fig. 8b).

When pressure data were used to obtain the *A*, *B*, and *C* matrices, again the system was found to be neither controllable nor observable, with only one input located at the tip of the delta wing, even though the scaled controllability and observability vectors look different in this case. These vectors, for the random gust excitation, are presented in Fig. 9. Note, however, that the 55 modes that appear here do not correspond to those of the VL model, or at least such a relationship was not established.

Modal controllability provides a measure of how difficult it may be to excite the respective mode by the input(s). For simplicity, and without losing generality, let us consider only one input located at the tip element of the wing. A weak modal controllability means that the considered mode is difficult to excite by the chosen input. One may consider selecting an input location or several locations that would produce a relatively stronger modal controllability for the modes of interest. In our example, shown earlier, it is seen that the dominant branch of the eigenvalues is least controllable in comparison with other branches of eigenvalues regardless of the locations of the excitation inputs. Nevertheless, eigenvalues in the dominant branch are the most observable. In SID both controllability and observability are equally important. A combination of weak controllability and strong observability may be sufficient to identify the eigenvalues (modes) of interest. A conventional measure of the modal identifiability is the product of the modal controllability and observability for the mode of interest. An experimentalist, before

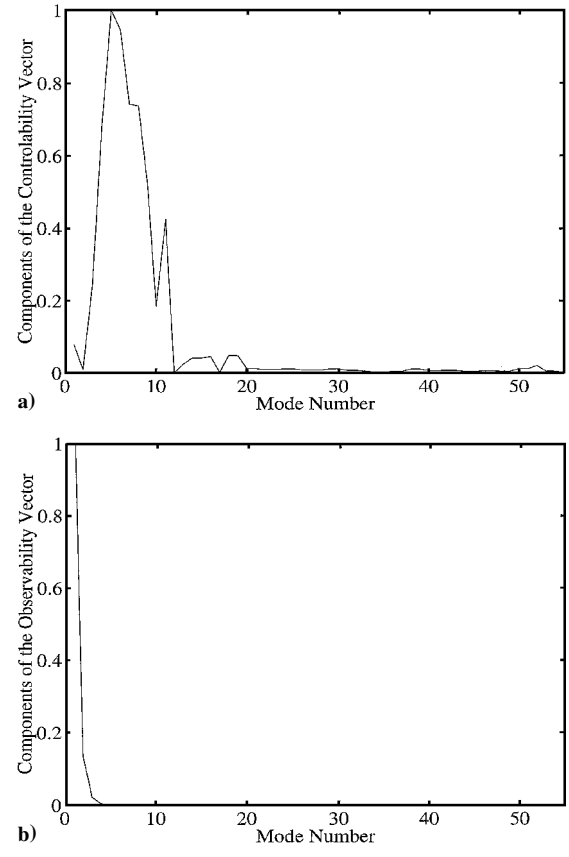

Fig. 9 Vector components of a) controllability and b) observability: Here *A*, *B*, and *C* matrices were identified from the pressure strength data when the wing was excited by the random gust; the only input is located at the tip of the delta wing.

designing and performing an experiment, may need to use an analytical state-space model to evaluate the modal identifiability for the modes of interest to choose proper locations for excitation inputs and measurement outputs. In addition, the excitation signal must be rich in frequency for the modes of interest to excite these modes properly.

Conclusions

A state-space representation of a theoretical VL model has been developed using an SID approach. The case of limited measurement data has been considered. This is done in anticipation of using the proposed SID method with experimental data, for example, an SID model might be obtained from pressure (sensor) measurements on a wing in a wind tunnel. Two possible SID approaches have been presented. Numerical results showed the importance of the choice of the wing motion or gust under consideration on building SID models and predicting the vortex strengths or pressure on a wing. Modal controllability and observability have been discussed. Numerical results for the chosen delta wing VL model have shown that the modes corresponding to the dominant branch of the eigenvalues of the flow are the least controllable and most observable. Least controllable means that these modes are difficult to excite by the type of downwash discussed in this paper, such as the step angle of attack, frozen sharp-edge gust, frozen gust of changing frequency, random downwash, or frozen random gust. On the other hand, most observable means that the dominant modes are easy to observe in terms of vortex strengths or the pressure distribution on the wing. Identifiability of modes depends clearly on both modal controllability and observability. The product of modal controllability and observability is commonly used as a measure of modal identifiability.

References

[1] Hall, K. C., "Eigenanalysis of Unsteady Flows About Airfoils, Cascades, and Wings," *AIAA Journal*, Vol. 32, No. 12, 1994, pp. 2426–2432.

[2] Tang, D., Kholodar, D., Juang, J.-N., and Dowell, E. H., "System Identification and Proper Orthogonal Decomposition Method Applied to Unsteady Aerodynamics," *AIAA Journal*, Vol. 39, No. 8, 2001, pp. 1569–1576.

[3] Juang, J.-N., *Applied System Identification*, Prentice–Hall, Englewood Cliffs, NJ, 1994, pp. 121–167.

C. Pierre
Associate Editor